Impact of silica pore structure on the performance of metallocene catalysts in ethylene gas-phase polymerization

Felipe Morais Bolner, Yashmin Rafante Blazzio, Bárbara Rezende Lara, Fabricio Machado, Timothy F L Mckenna

Impact of Silica Pore Structure on the Performance of Metallocene Catalysts in Ethylene Gas-Phase Polymerisation

Felipe Morais Bolner,[1,2] Yashmin Rafante Blazzio,[1] Bárbara Rezende-Lara,[1] Fabricio Machado,[2,3] and Timothy F. L. McKenna[1,*]

[1] Université de Lyon, Univ. Lyon 1, CPE Lyon, CNRS, UMR 5265, Laboratoire de Chimie Catalyse Polymères et Procédés (CP2M), LCPP team, Bât 308F, 43 Bd du 11 Novembre 1918, F-69616 Villeurbanne, France

[2] Chemical Engineering Program, Federal University of Goiás, 74690-900, Goiânia, GO, Brazil

[3] Institute of Chemistry, University of Brasília, *Campus* Universitário Darcy Ribeiro, 70910-900, Brasília, DF, Brazil.

Abstract:

Several commercial silicas were used to support metallocene active centres, and the resulting precatalysts were used to study the impact of the pore size and pore size distribution of the support on the polymerization kinetics and resulting polymer properties. Pore volume distribution played a major role in the fragmentation of silica-supported catalysts, where mesoporous silicas with a narrow distribution in the region obtained higher activities and faster fragmentation than silicas with a broad pore volume distribution. Therefore, it is shown that care must be taken when using standard information on particle porosity as this quantity can be misleading. It appears that the minimum pore size, particularly on the particle surface can be a very important parameter even if it does not impact the estimate of the porosity.

Author Information

* Corresponding Author: E-mail: timothy.mckenna@univ-lyon1.fr

1. Introduction

Metallocene catalysts supported on a suitable solid carrier are used industrially for several applications in low pressure slurry and gas phase ethylene polymerisation processes. [1-3] Among the various supports available, amorphous silica is by far the most commonly used material for this purpose because it is inexpensive, spherical, and has a balance of material properties needed for this type of application, including a high surface area and pore structure that can be tailored over a wide size range, proper mechanical properties to favor the catalyst fragmentation process, a controllable number of silanol functions on its surface that can be used to anchor catalyst and cocatalyst, and it can be "doped" to enhance catalyst activities.[4,5] Commercially available amorphous silica gel supports for metallocenes can be either a product of spray-drying or emulsion technology. Typically, the silica used for this purpose have pore volumes in the range of 1-3 $mL \cdot g^{-1}$, average pore diameters on the order of 10-30 nm, with particle sizes in the range of $1\text{-}10^2$ μm.[5]

It is widely accepted that the physical properties – particle size and porosity – of silica supports are as crucial as the chemical properties of their surface in determining catalyst performance. It is possible that they impact the distribution of the catalyst and co-catalyst throughout the support particles during catalyst synthesis, [6, 7] (co)monomer(s) diffusion during the polymerisation, molar mass of the polyolefin[8] and, last but not the least, crystallization process of nascent polyolefin chains within the porous support.[9] In addition, it is well known that how the surface is calcined can change the performance of a given catalyst in terms of the observed polymerisation rate.[10]

Earlier papers from our group discussed the impact of particle size on the rate of polymerisation and molar mass distribution (MMD).[11-13] It was shown that, for a given support and catalytic precursor, the rate of polymerisation decreased as the particle size increased, and that in certain cases, the average molar mass also decreased as the particles size increased. It was also briefly demonstrated that methylaluminoxane (MAO) impregnation can also be influenced by particle size, with larger particles requiring longer impregnation times that smaller ones.[11, 14] However, the porosity of the catalyst supports – also called texture by some authors – must also be important. Despite the interest and quality of many of these works, it is often the case that they

present an analysis that focuses on the pore volume distribution and ignores the fact that they are using many kinds of materials for supports, and do not control for the particle size distribution.

For instance, in two different studies Silveira et al.[15-17] studied ethylene homopolymerisation using metallocenes supported on Grace silicas, bare alumina, MCM-41, SBA-15, MCM-22, and non-conventional supports. Activities were found to be higher for the catalysts with larger final pore diameters, which were within 50 to 80 Å. The authors attributed this effect to the facilitated fixation of metallocenes inside of larger pores, along with easy access of MAO and monomer to the supported metallocene. The authors attributed low activities of the catalysts with low pore diameters to the possibility of the formation of inactive bidentate species. However, one needs to point out that the particle sizes of the supports used were also significantly different, and as discussed elsewhere the particle size also has a strong impact on observed activities.[12, 13]

In a similar study Jongsomjit et al.[18] studied the impact of support geometries using a variety of supports, and also saw higher activities with larger pore sizes. Nevertheless, they too ignored the influence of particle size. Also, as with the previous studies, it is very difficult to compare supports of a different chemical nature based only on the pore structure, since we have just seen that for similar calcination conditions, different supports with the same sites have different kinetics.

McDaniel[8] discussed the influence of pore structure on the fragmentation phenomenon of the catalyst support, stating that pore volume defines friability of the support, while pore diameter defines the mechanism of polymer growth from the pores. While these remarks were for chromium catalysts, there is no reason that this should not extend to other catalyst systems. This was also studied by Tisse et al,[12] who observed that silicas with small pore diameters (3.7 nm) had no activity at all. They concluded that it was possible that MAO (especially if it forms dimers or trimers) might block the pores of the support making them unavailable for monomer diffusion.

If we return to the concept of MAO impregnation of the catalyst supports, Smit et al.[19] compared two supports, Grace 948 and PQ MS3040. They observed that the calcination conditions, as well as differences in porosity, led to the formation of core-shell Al distributions in the catalyst particles. Bashir[20] also studied the same supports along with silica PQ MS1732 but also taking into account that PQ silicas present much more homogenous pore structures, while Grace presents interstitial voids that allow a better impregnation of MAO and metallocene.

Impregnation temperature might also be varied to obtain different graftings, as well as the washing method after grafting. Zheng[21] affirmed that at room temperature, uniform impregnation is hard to achieve, whereas Severn[22] observed evenly distributed aluminum atoms in the silicas activated with MAO at 130 °C for 3 hours. Tisse[14] observed higher activities for metallocene catalysts with MAO impregnation for 4 hours than the ones impregnated for 1 hour, both synthetized at 85 °C. Thus, impregnation time and temperature are variable in relation to the pore size distribution of the support used and to the final Al and metallocene distribution on the catalyst.

Therefore, in the present study we aim to investigate the impact of silica porosity on i) the distribution of metallocene/MAO catalyst inside the support particles, and ii) ethylene homopolymerisation in gas phase process in short times. As many studies focused on the impact of the porosity on the performance of silica supported metallocenes have been clear on whether the particle size was kept constant while changing silica porosity. Furthermore, the effect of the pore structure on catalyst and/or co-catalyst distribution inside the support particles does not appear to have been extensively analyzed in such studies. This point is of great importance when using a cocatalyst like MAO, which is bulky and has the tendency to agglomerate depending upon MAO/metallocene ratio[23] as well as on its age.[24]

2. Experimental section

2.1. Materials

Several commercial silicas were in this study, the physical characteristics of which are shown in **TABLE 1**. To obtain silica supports with well-defined particle sizes, the commercial silicas supplied by the Asahi Glass Company (AGC Si-Tech) were narrow enough in terms of size distribution that sieving was not necessary. Silica Grace Sylopol 948 was provided by Grace.

The metallocene precursors used to make supported catalysts were (*n*-BuCp)$_2$ZrCl$_2$, and *rac*-ethylene bis(4,5,6,7-tetrahydro-1-indenyl)zirconium dichloride – abbreviated to "THI" –, and both metallocenes were provided by Strem Chemicals Inc (Bischheim, France). Tri-isobutylaluminium (TIBA) was used as received from Witco Corporation. The MAO solution 29.4 wt% in toluene was supplied by Grace with the following characteristics: 13.3 wt% Al, 4.94

wt% $AlMe_3$, gas/Al = 1.65. Dry toluene and n-heptane used for catalyst synthesis were purified in four columns (three filters, MB-KOL-A, MB-KOL-M2, MB-KOL-M3, and a MB-KOL-C catalyst) in a MBraun SLS system prior to its use.

Ethylene with a nominal purity of 99.95% was purchased from Air Liquide (Paris, France), and passed through three different purification columns before use: a first one filled with reduced BASF R3-16 catalyst (CuO on alumina), a second one filled with molecular sieves (13X, 3 Å , Sigma-Aldrich), and a last one filled with Selexsorb COS (Alcoa). Finally, carbon dioxide with purity of 99.995% and nitrogen gas with purity of 99.999% were provided by Air Liquide (Paris, France).

2.3. Catalyst Synthesis Procedure

The incipient wetness method[25, 26] was used to prepare all the catalysts used in this work unless otherwise mentioned. All silicas were dehydroxylated at 600 °C overnight under dynamic vacuum of 10^{-3} to 10^{-5} mbar prior to their impregnation with the metallocene/MAO mixture. Dehydroxylations at 600 °C start with around 4 g of each silica left under 200 °C at a heating rate of 5 °C/min for 2 hours in a quartz Schlenk flask, followed by calcination at 600 °C under vacuum for over 12 hours. It should be noted that the dehydroxylation temperature of 600 °C was selected based on a detailed study done using the Grace 948 support as support for (*n*-$BuCp)_2ZrCl_2$.[10] There is no guarantee that this will be the optimal calcination procedure for the other supports, but for the sake of consistency the same procedure was used for all of the silica used in this study.

Two different incipient wetness catalyst synthesis methods were used for this study: a two-step and a three-step method. The first method was used for all (*n*-$BuCp)_2ZrCl_2$ catalysts, while most of the THI catalysts were synthetized using the three-step method.

For the first method, the first step starts by the mixing of a weighed amount of (*n*-$BuCp)_2ZrCl_2$, in dry toluene and MAO (30 wt% toluene solution), which are left for 1 hour under stirring at room temperature inside the glove box. The amounts of metallocene and MAO were selected by aiming Al/Zr molar ratio of 150 in the final catalysts, whereas the volume of toluene used was in 150 % excess of the pore volume of the used silica support. More precisely, the volume of the

MAO 30 wt% solution used per amount of silica was 1.77 mL/g for each catalyst. In the second step, the mixture containing $(n\text{-BuCp})_2ZrCl_2$, toluene and MAO was added dropwise to the weighed amount of dehydroxylated silica followed by heating at 50 °C for 1 h without any stirring. The supported catalyst was dried under vacuum at 75 °C, without applying any wash, for 2 to 3 h and then stored inside the glovebox.

The three-step incipient wetness method, also known as the SMAO method, consisted of synthetizing an activated silica prior to its metallocene grafting, and was used only for the THI-activated catalysts. For such, also 1.75 mL of the MAO solution per gram of dehydroxylated silica were mixed with 150 % of the silica pore volume in toluene, and then the resulting solution was added dropwise to the dehydroxylated silica in a Schlenk flask inside of a glovebox. The resulting slurry was heated at 80 °C for 4 hours under argon atmosphere without stirring, and afterwards the supernatant solution over the slurry was removed with a syringe. Dry heptane in the same volume of the removed toluene was inserted into the slurry to wash any unreacted MAO, then gently stirred by hand, and removed with a syringe. Lastly, the slurry was dried under vacuum at 80 °C for 2 hours. The resulting free-flowing white powder, henceforth called SMAO, was stored in a glovebox prior to its second step, the metallocene impregnation. Following an Al/Zr molar ratio of 150, a solution of the metallocene compound is prepared in pure dry toluene prior to its dropwise addition onto the SMAO, followed by heating at 50 °C for 1 hour, heptane wash and vacuum drying at 50 °C for at least 2 hours.

Catalysts activated by $(n\text{-BuCp})_2ZrCl_2$ were free-flowing orange powders, while the ones activated by THI were free-flowing yellow powders.

2.4. Stopped-Flow Polymerisation Protocol

The procedure for the nascent polymerisation study in gas-phase reactions in the membrane-like fixed-bed reactor (Annular Stopped Flow Reactors, ASFR) and a description of the device have been presented in detail by Blazzio et al.[27] Briefly, the ASFR is composed of concentric cylinders, with the internal cylinder being a fritted metal membrane filter, blocked at both ends by glass wool. A mixture of around 40 mg of catalyst and 1,500 mg of sodium chloride (NaCl) salt (purified by recrystallisation in acid citric solution, dried under vacuum at 200 °C for 5 h) is put in the annular space, the feed gas is heated to a desired reaction temperature and fed into the

central cylinder. The gas flows through the membrane, reacting with the catalyst in the annular space and then out to the exit lines. The reactors were filled in a glovebox and sealed with rubber septa before being installed in the ASFR set-up. The configuration of this device allows us to run 3 reactions at a time.

Ethylene homopolymerisations were carried out in reaction times of 15, 30, 45 and 90 seconds at ethylene mass flow of 986 g/h at 11 bar pressure (corresponding to a velocity of 20 cm/s). Inlet and outlet temperatures, reactor pressure, as well as flowrate of nitrogen – used as purge gas –, carbon dioxide – used as catalyst poison for reaction quenching –, and ethylene were collected using inline thermocouples, pressure transmitters and mass flowmeters, respectively, and acquired data were sent to a computer every 0.5 second. All the injections were set in the software interface and done automatically.

After each reaction, the reactors were weighed again to calculate reaction yield, and the mixture of sodium chloride and polyethylene was placed in a beaker and water was used to dissolve the salt bed, followed by filtration of the mixture using a polyvinylidene difluoride membrane and dried under vacuum at 70 °C for 3 hours before being kept in a sealed container for later analyzes. Activity curves were calculated according to the model described by Blazzio et al.[27]

2.5. Silica and Catalyst Characterization

Al and Zr content of the final catalysts were obtained by Inductively Coupled Plasma-Atomic Emission Spectroscopy (ICP-AES) at Mikroanalytisches Labor Pascher, Germany.

Nitrogen adsorption/desorption isotherms of silica and silica-supported final catalysts were obtained in a Micromeritics ASAP 2020 V3.04 H unit at -196 °C. All the silica samples were degassed for 4 h with no pre-heating. Specific surface areas were determined by the Brunauer–Emmett–Teller (BET) equation.[28] Desorption branch of Barrett–Joyner–Halenda (BJH) method[29] which employed Halsey standards was used to estimate the mesopore size and pore volume distribution of all the samples.

Scanning Electron Microscopy (SEM) and coupled Energy-Dispersive X-ray (EDX) with SEM were done for some supported catalysts samples. First, each sample was put on a doubled-sided conductive carbon adhesive tape priorly attached to a sampler. Then, the samples were put inside

of the vacuum chamber, which rotated them while they were metallized under vacuum with a 10 nm copper layer in a Bal-Tec MED-020 High Vacuum Coating System using 3 to 10 keV. In a ZEISS Merlin VP Compact microscope, the metallized samples were placed under vacuum, photographed, and had their particles diameters calculated using the SmartSEM software.

For the SEM-EDX analyzes, before being put under vacuum for their images acquirement, the samples were initially put in a low viscosity EpoFix resin, which was chemically hardened and then metallized and cut using a Diatome Ultra 45 diamond knife in a Reichert Ultracut S ultramicrotome.

2.7. Polymer Characterization

Thermal characterisations were performed via Differential Scanning Calorimetry (DSC) on a Mettler Toledo DSC 1 equipped with an auto-sampler and a 120-thermocouple sensor. The temperature and the heat flow of the equipment were calibrated with an indium standard. All samples were accurately weighed (between 5 to 10 mg) and sealed in 40 µL aluminum pans. They were heated from -20 °C to 180 °C at 10 °C min^{-1} with an empty 40 µL aluminum pan as reference. Two successive heating and cooling ramps with 5-minute intervals between the maximum and minimum temperatures were performed. Dry nitrogen gas with a flow rate set at 50 mL min^{-1} was used as the purge gas. Melting temperature (T_m) was measured at the top of the endothermic peak of the second heating ramp. The STAR^e thermal analysis software is used to calculate the melting temperature and the crystallinity (χ) of the polymers: $\chi = \Delta H_m / \Delta H_m^0$ where ΔH_m (J g^{-1}) is the second melting heat of the sample and ΔH_m^0 (293 J g^{-1}) the melting heat of a 100% crystalline polyethylene.

Finally, SEM and SEM-EDX were also performed for the polymer samples following the same aforementioned methods.

3. Results and Discussion

3.1. Supports and catalysts porosity studies

The properties obtained via nitrogen porosimetry and elemental analysis are shown in **TABLE 1**. The silica with lowest pore volume and diameter is S2, and its catalysts were the ones with the lowest pore volumes as well. Supports S2, S3 and S5 are very similar in their properties. Silica S4 had the biggest particle, and along with S1, presents the largest pore volumes and pore diameters of the studied supports. Finally, all catalysts had similar Al/Zr ratios independently on the support used and around the predicted values.

As mentioned before, it is important to keep the particle size of the silica support (and the resultant catalyst) constant while studying the impact of catalyst porosity on reaction kinetics and polyethylene properties. Since no stirring was applied during the catalyst synthesis, we can confidently assume that the final supported catalysts possess particle size distribution (PSD) like those of their parent silica fractions. In addition, the provider of the support showed that its silicas had PSD narrow enough not to require sieving.

TABLE 1 Nitrogen porosimetry and ICP-AES results of as-received commercial supports and their respective metallocene catalysts.

Silica	Support code	Surface Area (m^2/g)	Pore Volume (cm^3/g)	Pore Diameter (nm)	d_{50} (µm)	Metallocene type	Catalyst Code	Surface Area (m^2/g)	Pore Volume (cm^3/g)	Pore Diameter (nm)	Al (%wt)	Zr (%wt)	Al/ Zr
		Support properties						**Catalyst properties**					
DM-L-303	S1	296	2.2	30	32	THI	S1-a	327	1.11	17.6	14.2	0.24	200
						(n-BuCp)$_2$ZrCl$_2$	S1-b	265	0.77	18.0	14.3	0.23	210
DM-H-302	S2	618	1.7	11	35	THI	S2-a	294	0.47	10.4	15.1	0.26	196
						(n-BuCp)$_2$ZrCl$_2$	S2-b	188	0.33	12.0	13.9	0.22	214
DM-M-302	S3	580	1.8	13	35	THI	S3-a	371	0.72	11.4	16.9	0.24	238
						(n-BuCp)$_2$ZrCl$_2$	S3-b	315	0.75	14.2	14.4	0.24	203
DM-L-403	S4	363	2.1	23	43	THI	S4-a	326	0.82	12.1	16.9	0.26	220
						(n-BuCp)$_2$ZrCl$_2$	S4-b	217	0.61	12.2	14.6	0.24	206
M-302-F	S5	500	1.8	15	30	(n-BuCp)$_2$ZrCl$_2$	S5-a	330	0.76	13.9	14.4	0.35	139

Another way to observe the original silica morphology integrity on the catalysts is the nitrogen sorption plots, as shown in **FIGURE 1** and **FIGURE 2**.

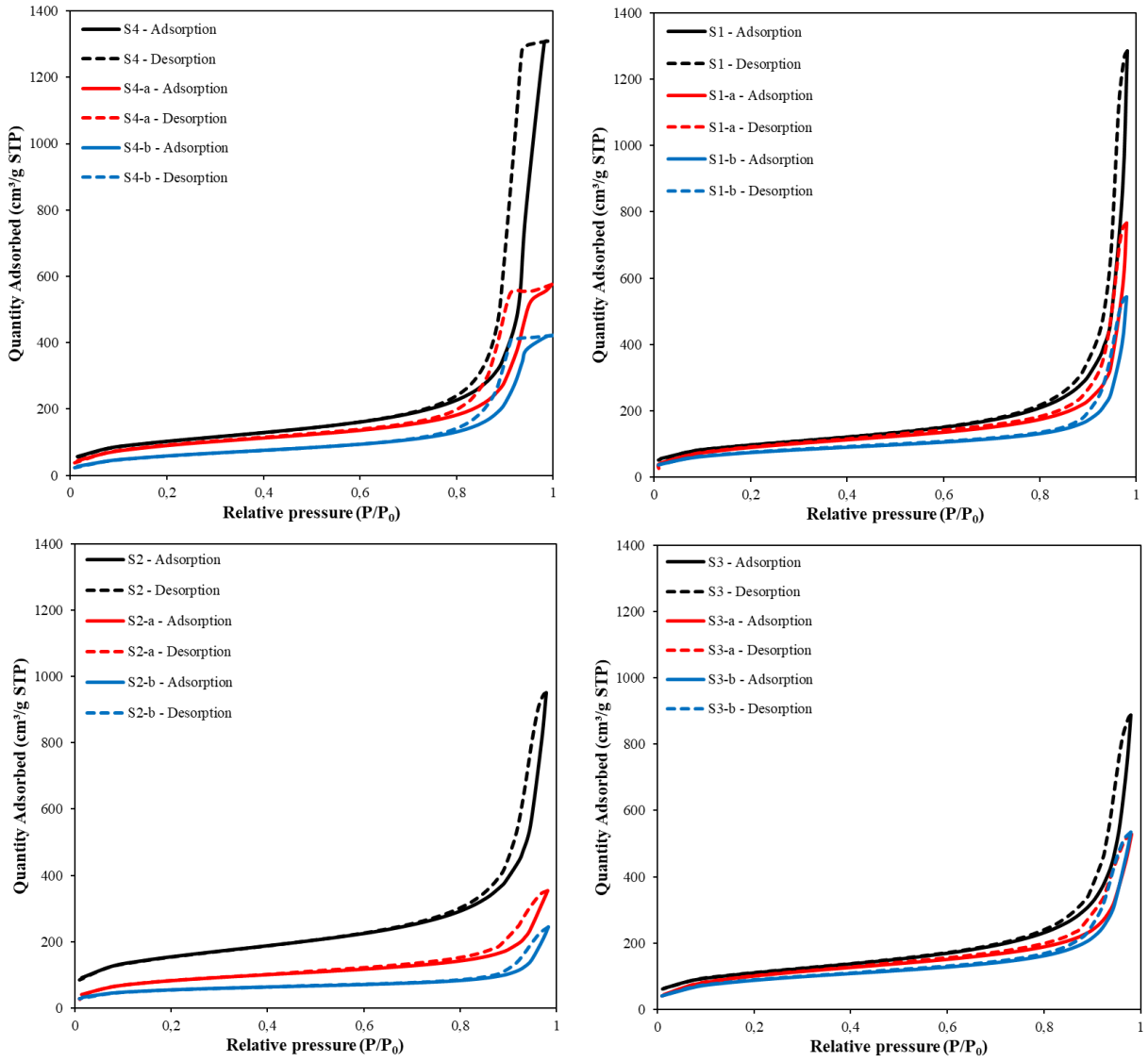

FIGURE 1 Sorption isotherms for the dehydroxylated silicas and their corresponding supported metallocene catalysts, as described in **TABLE 1**.

Particle integrity can be shown by the maintenance of the shape of the sorption isotherms of the original supports in their resulting catalysts. This was also expected from the chosen synthesis methods since no stirring was used for both methods. In addition, one can also see the partially occupied pores in the catalysts by the lower amounts of adsorbed nitrogen compared to their original dehydroxylated silicas. However, it is also visible that silicas S4 and S1 had around the

same values of maximum nitrogen gas sorption, with a difference in the shape of their curves. Silicas S2 and S3 had also very similar sorption curves with similar adsorbed nitrogen amounts.

The presence of hysteresis in all sorption curves is an indication of their mesoporous nature. Nevertheless, a very clear difference in these curves is seen when comparing S4 silica and its catalysts to the other supports. S4, S4-a, and S4-b present a desorption plateau instead of the smoother transition from adsorption and desorption seen in the other silicas.[30] The reason for this plateau is its narrow pore volume distribution, as shown in **FIGURE 2**.

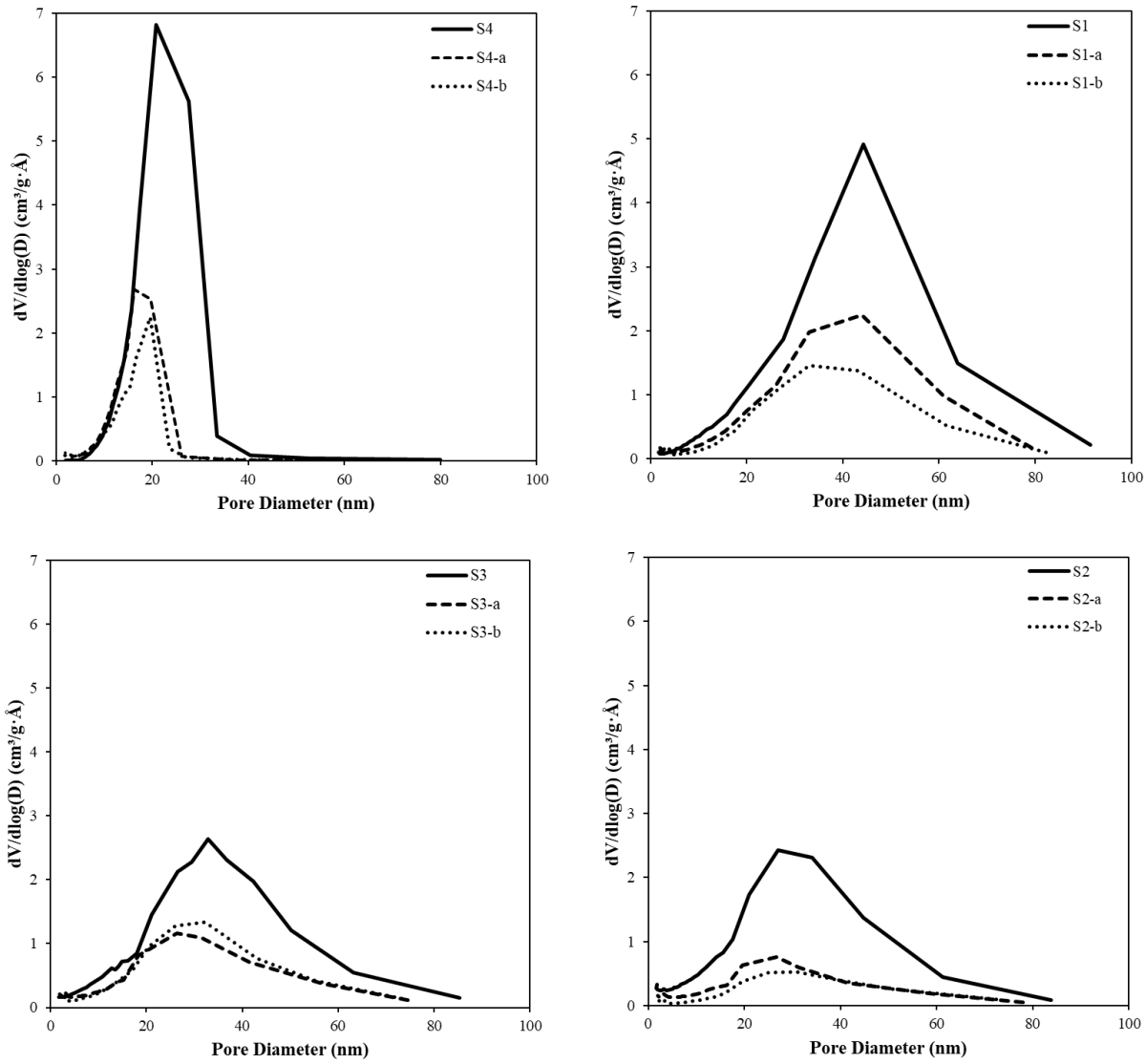

FIGURE 2 Pore volume distributions for the dehydroxylated silicas and their corresponding supported metallocene catalysts.

From **FIGURE 2** one can see that, though silicas S1 and S4 present almost the same average pore volume, their pore volume distributions are very different, with S1 presenting a much broader distribution. Only S4 from the four silicas studied presented a narrow pore volume distribution, with no significant porosity after 40 nm, while the rest of the silicas showed wider pore volume distributions that go up to 90 nm. This indicates that, different from the other three silicas, S4 is more homogeneous, with similar pore diameters distributed from the surface to the core of its particles.

Silicas S2 and S3, as expected from their nitrogen adsorption-desorption curves, show resembling pore distribution profiles. On the other hand, this time we can also observe a slight bimodal pore distribution for both, in which a smaller pore diameter population that peaks around 14 nm merges with the main population around 30 nm. In addition, though S1 also had a wide pore volume distribution, it has larger pores than S2 or S3, as seen from its larger peak in **FIGURE 2** and higher amounts of adsorbed nitrogen in **FIGURE 1**.

Finally, for all silicas and their correspondent catalysts, it is seen smaller pore diameters than their original treated supports, indicating the partial filling of the pores with the grafting of cocatalyst and metallocene. It must be added also that a shift in the pore volume distribution to smaller pore diameters was observed for all catalysts in relation to their original supports, which indicates that bigger pores were the ones most filled with MAO and zirconocene.

3.2. Effect of Catalyst Porosity on the Nascent Morphology and Kinetics of Gas Phase Ethylene Homopolymerisation

The kinetics calculated via the inlet and outlet temperatures of the gases in the ASFR system are shown in **FIGURE 3**:

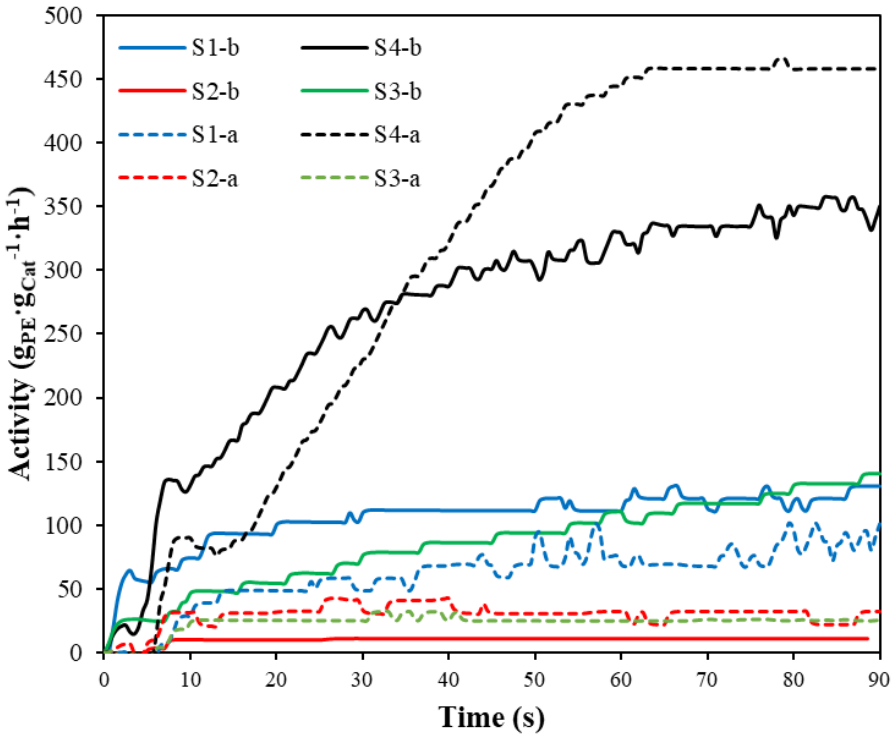

FIGURE 3 Instantaneous activity profiles over reaction time during the 90-second reactions in the ASFR system.

The activity profiles seen in **FIGURE 3** display three different kinetic behaviours: a very fast one for catalysts S4-a and S4-b; a rapid for S1-a, S1-b, and S3-b; and a slow and gradual S3-a, S2-b, and S2-a. One can see that, comparing these profiles with **FIGURE 2**, it was not the metallocene, but the porosity of the support the variable that produced the highest effect in the catalytic activities in the early stages of polymerisation. In general, the catalysts with narrow distributions, S4-a, S4-b, had higher activities than the ones with broad distributions. This occurred since the S4-supported catalysts were supported from shell to core since the silica has a very homogenous pore volume distribution. On the other hand, it is also visible that the THI catalysts – represented by the dashed lines – had higher activities than its (*n*-BuCp)$_2$ZrCl$_2$ counterparts – represented by the solid lines – with the exception for S2-supported catalysts. The activity profiles of the other reaction times – presented in **FIGURES S1**, **S2** and **S3** in Supporting Information – show pore effect much more pronounced and visible in the kinetics after 45 seconds of reaction.

FIGURE 4 shows yields over time in kg_{PE}/mol_{Zr}, displaying a growing yield with time in practically all the reactions, with exception for a small deviation presented by S2-a catalyst (THI/MAO/S2) from 45 to 90 s. Catalysts S4-a and S4-b appear to highly increase activity from

45 to 90 seconds of reaction, while the other catalysts seem to present a gradual increase of yield over time. In general, yields were very similar up to 45 s, and after 90 s the highest yields were obtained by the S4-supported catalysts.

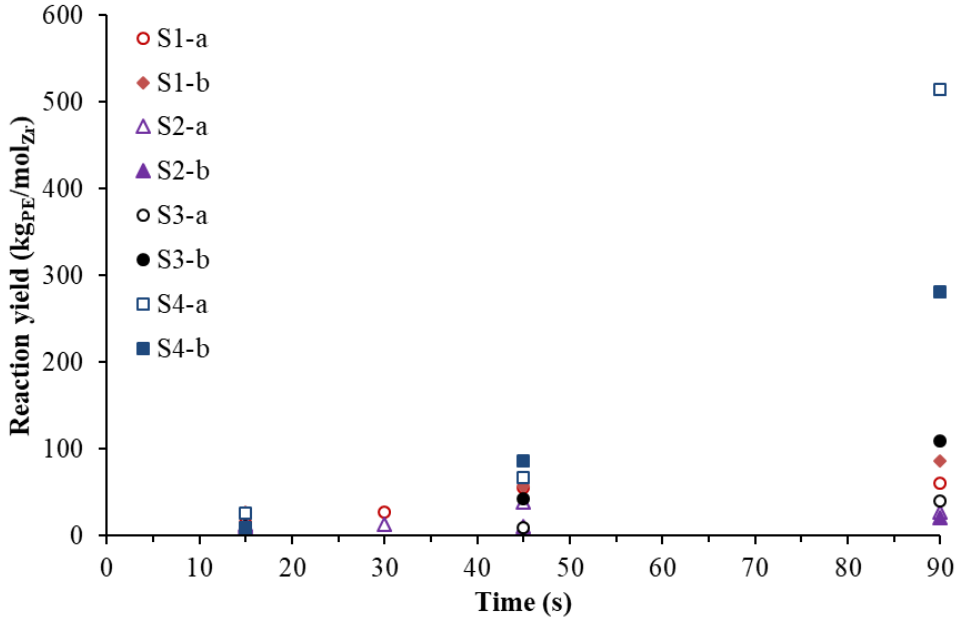

FIGURE 4 Yields over reaction time for all ASFR reactions.

TABLE 2 Crystallinity results via DSC for ASFR polymers.

	χ (%)							
	S1-a	**S2-a**	**S3-a**	**S4-a**	**S1-b**	**S2-b**	**S3-b**	**S4-b**
90 s	36.4	20.9	20.8	53.4	28.3	29.5	36.3	40.9
45 s	27.7	22.8	13.7	30.5	21.8	25.1	26.5	20.8
30 s	19.1	19.2	–	–	–	–	–	–
15 s	13.9	12.8	–	29.8	13.7	14.4	6.8	17.0

The second melting temperatures obtained are within the normal range for HDPE samples,[31] but are due to the evolution of the polymerisation. Catalyst fragmentation is also seen in **FIGURE 5** and **FIGURES S4-S7**, where the presence of bi- and tri-modality in the crystallization curves are due to the pore confinement mechanism in the first seconds of reaction, as seen in other works using Stopped-Flow reactors[32-34]. Di Martino et al.[35, 36] attribute this phenomenon in short-time

slurry-phase ethylene homopolymerisation using Ziegler-Natta catalysts supported on magnesium chloride to the initial high rates of polymerisation producing disordered and entangled chains.

Furthermore,

TABLE 2 shows a growing crystallinity over reaction time. S4-a and S4-b have consistently higher crystallinities than the other catalysts. This implies once more that they have less polymer formed in confined spaces at a given time and that fragmentation was faster. Once again, when looking at the two metallocenes separately, S1- and S4-supported catalysts presented the highest crystallinities for the THI metallocene, while for metallocene (*n*-BuCp)$_2$ZrCl$_2$ this difference becomes only visible for S4. This can be explained by *in-situ* hydrogen production of (*n*-BuCp)$_2$ZrCl$_2$ during ethylene polymerization, a property that the THI metallocene does not present.[20]

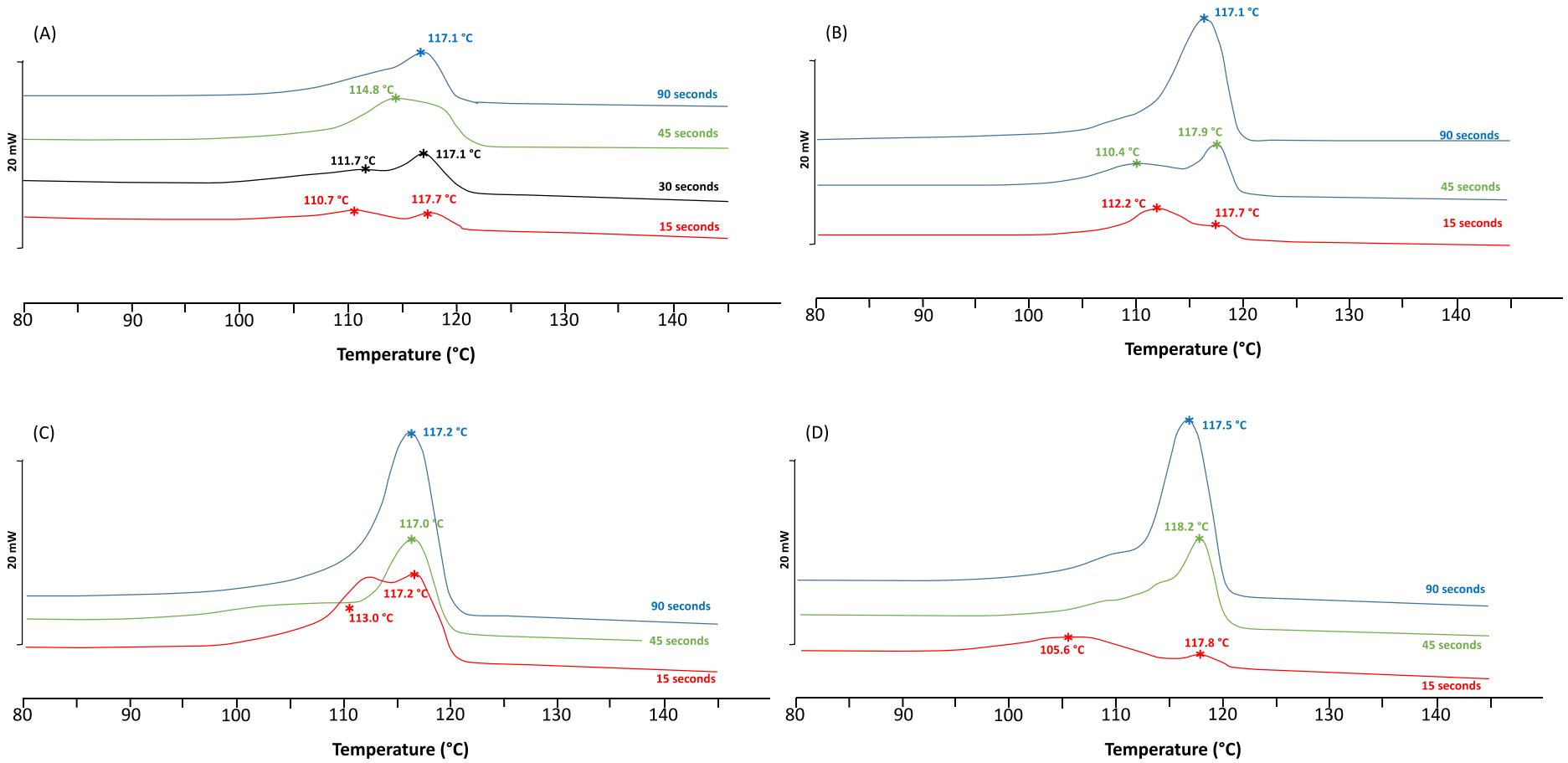

FIGURE 5 Crystallization profiles in the ASFR system for catalyst (A) S2-a, (B) S2-b, (C) S4-a, and (D) S4-b.

The evolution on the crystallization and melting profiles was seen for all studied catalysts. Though reaction times were not short enough for the visualization of a first crystallization peak at 75 °C as suggested in the literature, a second and the third ones in the regions around 105-115 °C can be seen in all studied samples. In addition, the second peak gives place to the third one in all cases, where the second peak loses its initial predominance at 15 seconds and, by 90 seconds, it is mostly consumed, indicating the chains are no more confined after this reaction time. In some cases, usually at 45 seconds, one can observe from two to three simultaneous and/or overlapping peaks – around 111, 114 and 118 °C – such as seen in **FIGURES S4** to **S7** in **Supporting Information**.

Catalysts supported in silicas S2 and S3 presented a slower evolution of these peaks, while silicas S1 and S4 presented a faster crystallinity evolution towards a more resolved peak, specially the ones supported on S4. This might suggest that the presence of larger pores lowered the pore confinement effect like seen in the small-pored silicas, where a bimodal crystallization could be seen up to 45 seconds. To further our studies, we selected two THI-activated catalysts for SEM-EDX, S4-a and S2-a, as depicted in **FIGURE 10**.

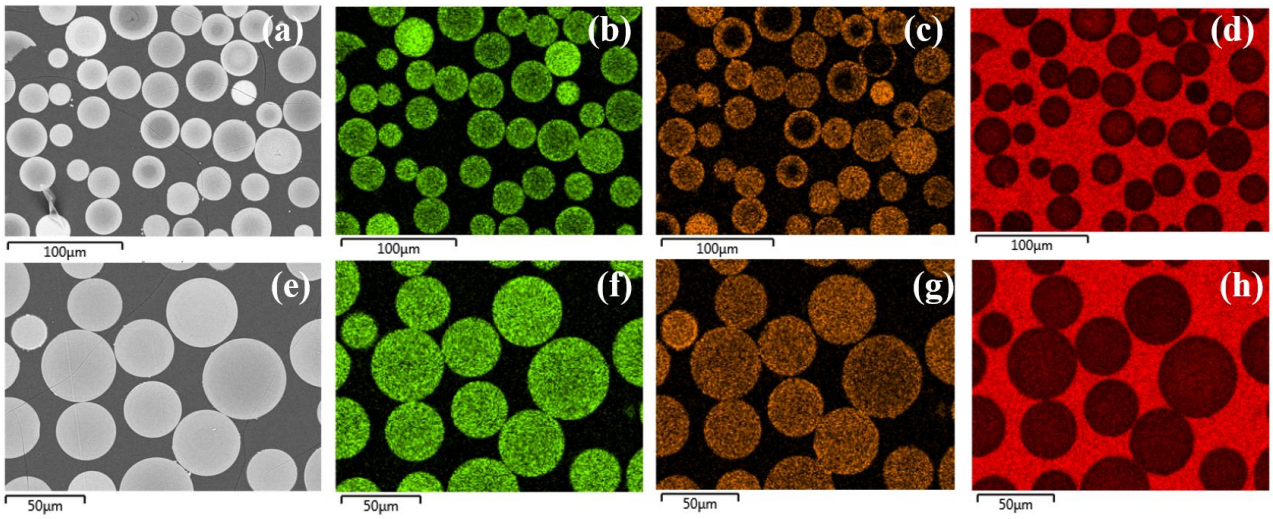

FIGURE 6. SEM-EDX images for cross section of catalysts S2-a (upper row) and S4-a (lower row). Original image (a and e); and silicon (b and f, in green), aluminum (c and g, in orange) and carbon (d and h, in red) distributions.

In these images, the intensity of the color indicates the density or concentration of the atom observed via X-rays. When analyzing the first images for S2-a and S4-a – **Figures 6A** and **6E** respectively – one can observe that S4-a particles present a more homogenous appearance, with

mostly the same grey color from their cores to shells; meanwhile, S2-a has very different particles with different densities, many of them presenting a brighter grey color on their shells than their cores. Their Si atom distributions – **Figures 6B** and **6F** – corroborate with this observation: silica S4 presents a more even distribution of pores from the outside to the inside of all particles, and silica S2 presents a packed shell and more porous core, with major Si density discrepancies between particles.

Furthermore, the very different Al distributions seen in **FIGURE 6C** and **Figure 6G** are, however, related to their differences in MAO impregnation. Due to their very large size, the MAO molecules will have their diffusion restricted inside small pores, requiring longer impregnation times during the catalyst synthesis to reach inner pores of the support – as also shown in **Figure S8** of the **Supporting Information**. Thus, considering the same synthesis method and MAO impregnation time, certain particles of small-pored catalysts might present no active sites whatsoever in its innermost pores, for it is required the presence of both MAO and zirconocene for their formation; meanwhile, catalysts with evenly distributed mesopores will present an even Al distribution from its surface to its core. This also explain why S1-a and S4-a, though supported in silicas with very similar average pore geometries, obtained different productivities and kinetic profiles – as also explained by their pore volume distributions in **FIGURE 2**. The carbon distributions – **FIGURES 6D** and **6H** in red – show nothing in particular, since no polymerisation reaction had been done for these particular samples but serve as references for the SEM-EDX images showed in **FIGURES 7** and **8**. It should be noted that one would ideally like to know how the pore size influenced the zirconium distribution. Unfortunately, the Zr signal was not strong enough to detect because of the very low levels of the active metal on the site. Even multiplying its concentration by an order of magnitude was not enough to allow for reliable detection of the metal.

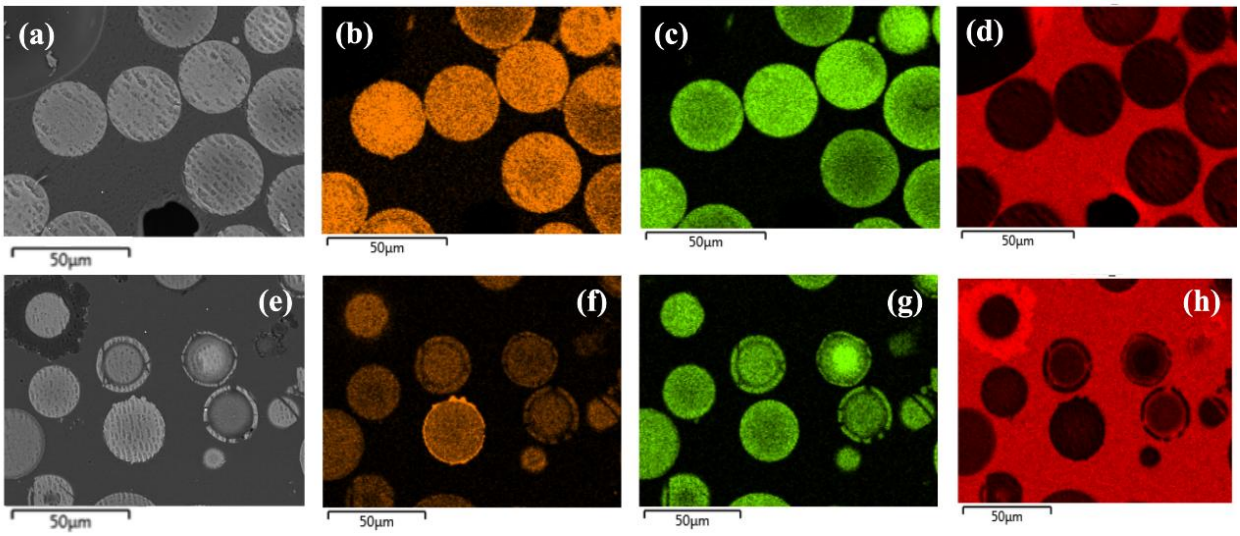

FIGURE 7 SEM-EDX images for cross section of S2-a after reactions with the ASFR for (upper row) 15 seconds and (lower row) 90 seconds. Original image (a and e); and silicon (b and f, in green), aluminum (c and g, in orange) and carbon (d and h, in red) distributions.

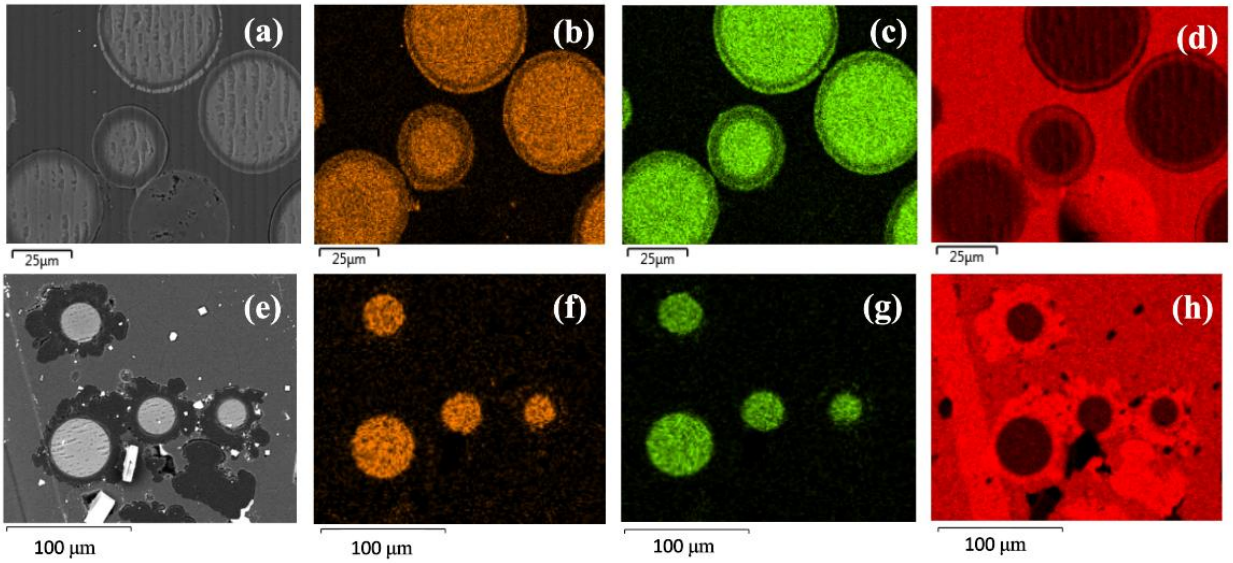

FIGURE 8 SEM-EDX images for cross section of S4-a after reactions at the ASFR for (upper row) 15 seconds and (lower row) 90 seconds. Original image (a and e); and silicon (b and f, in green), aluminum (c and g, in orange) and carbon (d and h, in red) distributions.

FIGURES 7 and **8** show the development of the polymerisation reactions over time. Again, the intensity of the color is proportional to the concentration of the related compound in the sample. The S2-supported catalyst presented slower particle growth than the S4-supported one. Observing **Figure 7A** to **7D** and **8A** to **8D**, 15-second reactions, the formation of a fragmented layer of catalyst is clear in the images of catalyst S4-a but not observed for catalyst S2-a particles. After

90 seconds of reaction, as shown in **Figures 7E** to **7H** and **8E** to **8H**, one can see a faster particle growth for catalyst S4-A, as the outer layer of the catalyst particles are surrounded by polymer (seen in brighter red color around the dark round particles). On the other hand, S2-a presents most of its particles in the first stages of growth at 90 seconds.

Furthermore, the differences in fragmentation can be attributed to the evenly distributed Al in the S4-a catalyst, which allowed this catalyst to homogenously anchor the zirconocene and, therefore, had active sites from its shell to its core, thus obtaining higher activities during the first seconds of reaction. On the other hand, the core-shell Al distribution of the S2-a catalyst produced particles with an uneven distribution of active sites, producing particles with high amounts of unfilled pores and, therefore, a catalyst with low activities.

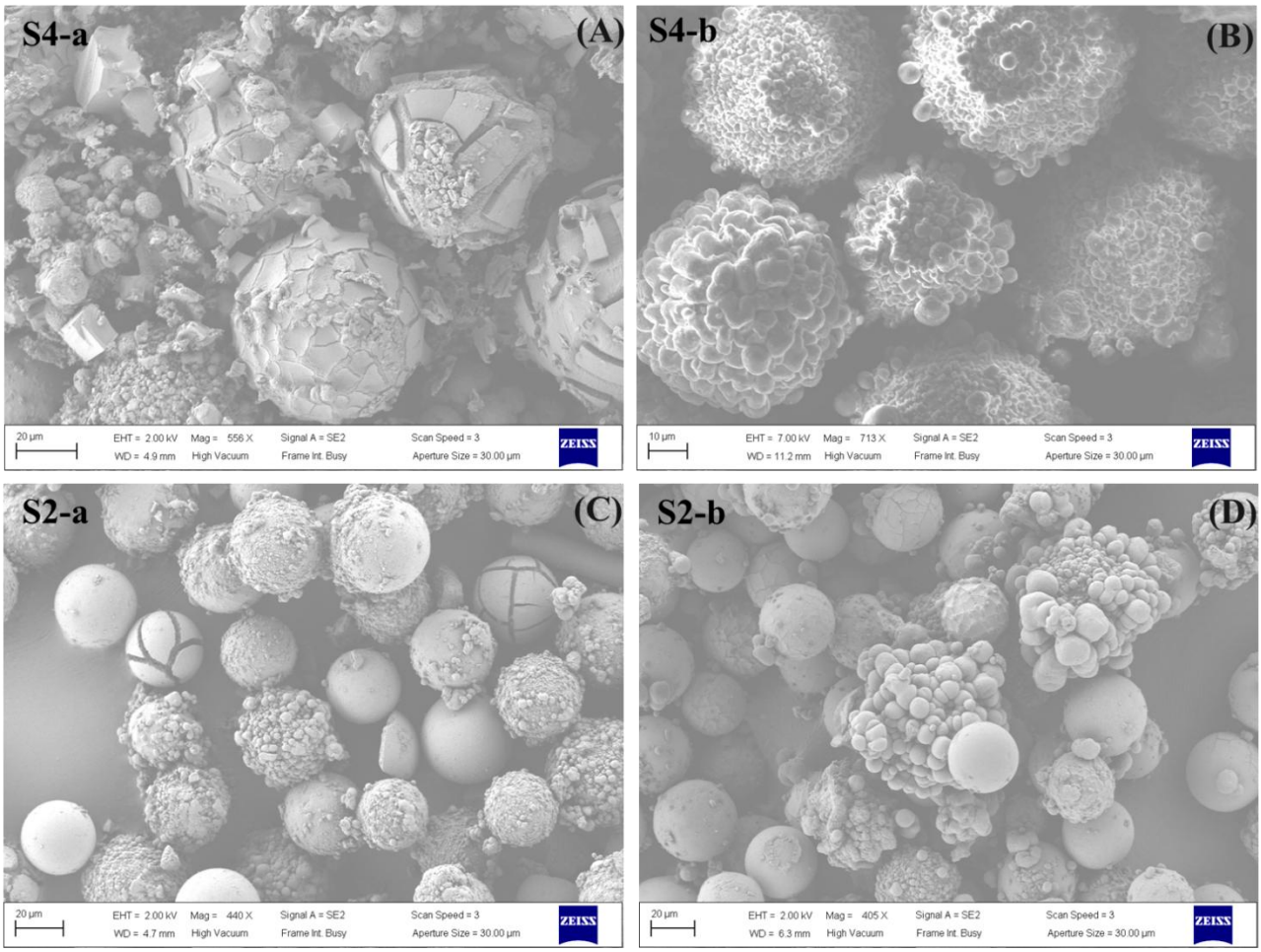

FIGURE 9 SEM photographs of 90-second reactions of (A) S4-a, (B) S4-b, (C) S2-a, and (D) S2-b catalysts.

S2-supported catalysts – **Erreur ! Source du renvoi introuvable.9C** and **9D** – still had unreacted catalyst particles in between reacted ones, while mostly polymer particles could be seen for catalyst S4-b – **Erreur ! Source du renvoi introuvable.10A** and **10B**. Comparing **FIGURE 3** to **FIGURE 9**, this can be attributed once more to the pore confinement effect. The larger pores caused lower mass transfer resistance and fast fragmentation on the initial seconds of reaction, followed by a decrease in the fragmentation rate caused by the filling of the pores with polymer. In the case of catalyst S4-a, one can see that, due to its very pronounced activity from the initial stages of polymerisation, the polymer particle did not reproduce the original morphology of the support. This suggests that the hydraulic pressure caused by the growth of polymer chains inside or the pores of the support was higher than the adhesive tension of the polymer on the fragmented parts of the support.

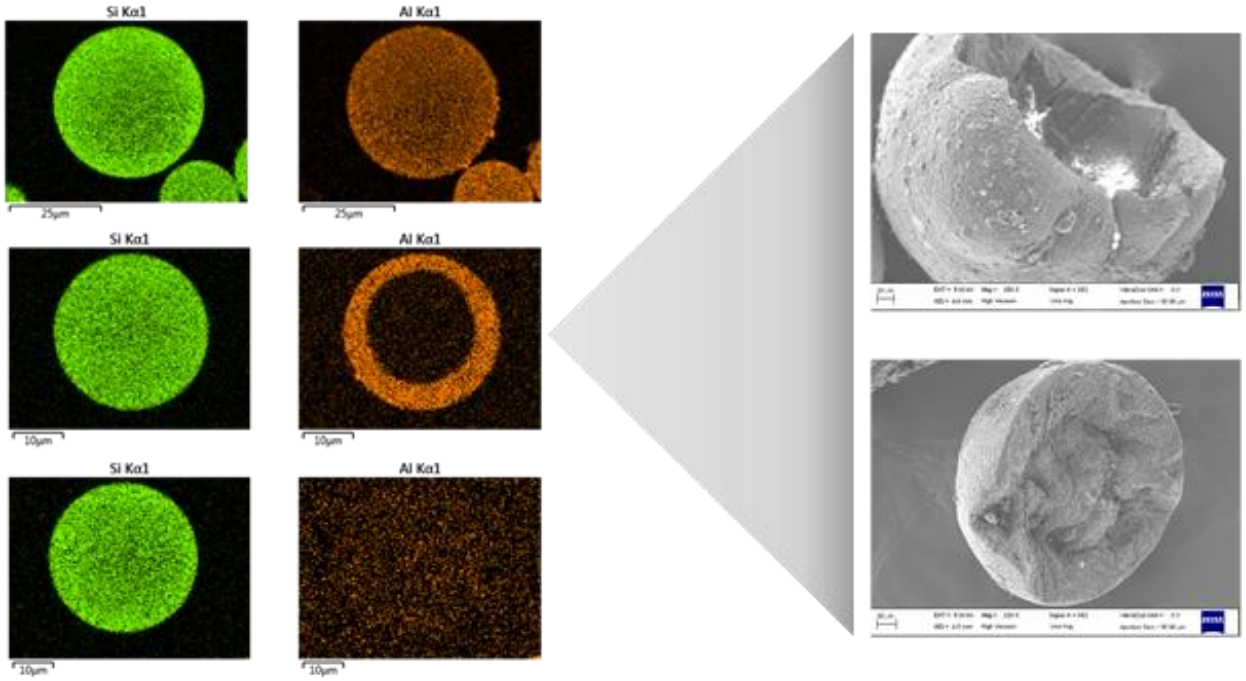

FIGURE 10. SEM-EDX of catalyst S5-a particles (left, in green and orange) and SEM of polymer particles it produced in gas-phase ethylene homopolymerisation (right, in grey).

Last, catalyst S5-a, such as S2-a, also displays different lack of homogeneity on the Al distribution. **FIGURE 10** shows three types of catalyst particles observed for the same batch of supported catalyst: a particle with evenly distributed active sites; a particle with a core-shell distribution of sites; and a catalyst with very low concentration of sites. In addition, the SEM

image of the polymer produced with S5-a shows the formation of hollow polymer particles due to the presence of core-shell Al distribution in the S5-a catalyst.

4. Conclusion

Silica pore morphology and dimensions can have a significant impact on the distribution of metallocene/MAO mixture throughout the particles. Ethylene polymerisation kinetics are also dependent upon silica support porosity. Silica-supported (*n*-BuCp)$_2$ZrCl$_2$/MAO and THI/MAO catalysts of equal particle sizes but different porosities (i.e., pore volumes, pore diameters and surface areas) evaluated in short time gas-phase ethylene homopolymerisation reveal that pore diameter and pore volume seem to significantly impact the instantaneous activity of the catalysts in both types and phases of polymerisations in a similar fashion. Higher activation rates were observed for the supported catalysts when the internal and external morphology of the catalyst particles was kept similar along with particle size. Since the level of mass transfer resistance can be assumed constant due to same particle sizes, this observation can be attributed to the slow fragmentation rate of catalysts with broad pore volume distributions observed by microscopy and porosimetry, as compared to that with homogenous and narrow pore volume distribution. The same effect of difference in pore volumes was noticed when two catalysts having different metallocenes were evaluated. With respect to surface area of the catalysts, no clear trend was observed.

Acknowledgements

The authors gratefully acknowledge the financial support Asahi Glass Company (AGC Si-Tech, Tokyo, Japan), and thank MI for discussions and his availability. FM thanks Conselho Nacional de Desenvolvimento Científico e Tecnológico (CNPq) and Coordenação de Aperfeiçoamento de Pessoal de Nível Superior (CAPES). All authors kindly thank Dr. Niyi B. Ishola for the help given with the MATLAB code used for the ASFR activity calculations, and Pierre-Yves Dugas with the help given during the SEM-EDX samples preparation.

REFERENCES

1. Stürzel, M.; Mihan, S.; Mülhaupt, R., From Multisite Polymerization Catalysis to Sustainable Materials and All-Polyolefin Composites. *Chemical Reviews* **2016,** *116* (3), 1398-1433.

2. Krallis, A.; Kanellopoulos, V.; Ali, M. A.-h., Comprehensive Study of Reactants Depletion in Catalytic Olefin Polymerization Industrial Loop Reactors. *Industrial & Engineering Chemistry Research* **2015,** *54* (33), 8247-8254.

3. Qiao, J.; Guo, M.; Wang, L.; Liu, D.; Zhang, X.; Yu, L.; Song, W.; Liu, Y., Recent advances in polyolefin technology. *Polymer Chemistry* **2011,** *2* (8), 1611-1623.

4. Duchateau, R., Incompletely Condensed Silsesquioxanes: Versatile Tools in Developing Silica-Supported Olefin Polymerization Catalysts. *Chemical Reviews* **2002,** *102* (10), 3525-3542.

5. Severn, J. R., Methylaluminoxane (MAO), Silica and a Complex: The "Holy Trinity" of Supported Single-Site Catalyst. In *Tailor- Made Polymers*, Severn, J. R.; Chadwick, J. C., Eds. Wiley- VCH Verlag GmbH & Co. KGaA: Weinheim, 2008; pp 95-138.

6. Nooijen, G. A. H., Ziegler/Natta catalysts in particle form ethylene polymerization: The effect of polymerization start-up on catalyst activity and morphology of the produced polymer. *Catalysis Today* **1991,** *11* (1), 35-46.

7. Nooijen, G. A. H., On the importance of diffusion of cocatalyst molecules through heterogeneous ziegler/natta catalysts. *European Polymer Journal* **1994,** *30* (1), 11-15.

8. McDaniel, M. P., Influence of Catalyst Porosity on Ethylene Polymerization. *ACS Catalysis* **2011,** *1*, 1394–1407.

9. Tioni, E.; Broyer, J. P.; Monteil, V.; McKenna, T. F. L., Influence of Reaction Conditions on Catalyst Behavior during the Early Stages of Gas Phase Ethylene Homo- and Copolymerization. *Ind. Eng. Chem. Res.* **2012,** *51*, 14673−14684.

10. Bashir, M. A.; Vancompernolle, T.; Gauvin, R. M.; Delevoye, L.; Merle, N.; Monteil, V.; Taoufik, M.; McKenna, T. F. L.; Boisson, C., Silica/MAO/(*n*-BuCp)$_2$ZrCl$_2$ catalyst: effect of support dehydroxylation temperature on the grafting of MAO and ethylene polymerization. *Catalysis Science & Technology* **2016**, 2962 –2974.

11. Tisse, V. F.; Briquel, R. M.; McKenna, T. F. L., Influence of Silica Support Size on the Polymerisation of Ethylene Using a Supported Metallocene Catalyst. *Macromolecular Symposia* **2009,** *285*, 45-51.

12. Tisse, V. F.; Prades, F.; Briquel, R. M.; Boisson, C.; McKenna, T. F. L., Role of Silica Properties in the Polymerisation of Ethylene Using Supported Metallocene Catalysts. *Macromolecular Chemistry and Physics* **2010,** *211*, 91-102.

13. Bashir, M. A.; Monteil, V.; Boisson, C.; McKenna, T. F. L., Experimental proof of the existence of mass-transfer resistance during early stages of ethylene polymerization with silica supported metallocene/MAO catalysts. *AIChE Journal* **2017,** *63* (10), 4476-4490.

14. Tisse, V. F. Kinetics and morphology of metallocene catalysts used in ethylene polymerisation. Université Claude Bernard Lyon 1, Lyon, 2006.

15. Silveira, F. L. d.; Petry, C. F.; Pozebon, D.; Pergher, S. B. C.; Detoni, C.; Stedile, F. C.; dos Santos, J. H. Z., Supported metallocene on mesoporous materials. *Applied Catalysis A: General* **2007,** *333* (1), 96-106.

16. Silveira, F.; Alves, M. d. C. M.; Stedile, F. C.; Pergher, S. B. C.; dos Santos, J. H. Z., The Role of the Support in the Performance of Grafted Metallocene Catalysts. *Macromolecular Reaction Engineering* **2009,** *3*, 139–147.

17. Silveira, F.; Alves, M. d. C. M.; Stedile, F. C.; Pergher, S. B.; Rigacci, A.; dos Santos, J. H. Z., Effect of the silica texture on the structure of supported metallocene catalysts. *Journal of Molecular Catalysis A: Chemical* **2009,** *298* (1), 40-50.

18. Wongwaiwattanakul, P.; Jongsomjit, B., Copolymerization of ethylene/1-octene via different pore sized silica-based-supported zirconocene/dMMAO catalysts. *Catalysis Communications* **2008,** *10* (1), 118-122.

19. Smit, M.; Zheng, X.; Loos, J.; Chadwick, J. C.; Koning, C. E., Effects of methylaluminoxane immobilization on silica on the performance of zirconocene catalysts in propylene polymerization. *Journal of Polymer Science Part A: Polymer Chemistry* **2005,** *43* (13), 2734-2748.

20. Bashir, M. A.; McKenna, T. F. L., Reaction Engineering of Polyolefins – The role of catalyst supports in ethylene polymerization on metallocene catalysts In *Polymer Reaction Engineering of Dispersed Systems*, Pauer, W., Ed. Springer: Cham, 2016; Vol. 1.

21. Zheng, X.; Smit, M.; Chadwick, J. C.; Loos, J., Fragmentation Behavior of Silica-Supported Metallocene/MAO Catalyst in the Early Stages of Olefin Polymerization. *Macromolecules* **2005,** *38*, 4673-4678.

22. Severn, J. R.; Chadwick, J. C.; Duchateau, R.; Friederichs, N., "Bound but Not Gagged" - Immobilizing Single-Site r-Olefin Polymerization Catalysts. *Chemical Reviews* **2005,** *105* (11), 4073-4147.

23. Babushkin, D. E.; Brintzinger, H.-H., Activation of Dimethyl Zirconocene by Methylaluminoxane (MAO) Size Estimate for Me-MAO$^-$ Anions by Pulsed Field-Gradient NMR. *Journal of the American Chemical Society* **2002,** *124* (43), 12869-12873.

24. Zijlstra, H. S.; Harder, S., Methylalumoxane – History, Production, Properties, and Applications. *European Journal of Inorganic Chemistry* **2015,** *2015* (1).

25. Bingel, C.; Goeres, M.; Fraaije, V.; Winter, A. Supported catalyst system, method for the production and use thereof in olefin polymerization. 3/9/2003, 2002.

26. Schottek, J.; Kratzer, R.; Winter, A.; Fraaije, V.; Brekner, M. J.; Oberhoff, M. Metallocene compound and polymerization catalyst comprising heterocyclic group. 22/10/2000, 2002.

27. Blazzio, Y. R.; Norsic, S.; Sheibat-Othman, N.; McKenna, T. F. L., Polymerization of ethylene in the gas phase—A new combined hardware and software tool. **2022,** *100* (9), 2491-2504.

28. Brunauer, S.; Emmett, P. H.; Teller, E., Adsorption of Gases in Multimolecular Layers. *Journal of the American Chemical Society* **1938,** *60* (2), 309-319.

29. Barrett, E. P.; Joyner, L. G.; Halenda, P. P., The Determination of Pore Volume and Area Distributions in Porous Substances. I. Computations from Nitrogen Isotherms *Journal of the American Chemical Society* **1951,** *73*, 373-380.

30. Thommes, M.; Kaneko, K.; Neimark, A. V.; Olivier, J. P.; Rodriguez-Reinoso, F.; Rouquerol, J.; Sing, K. S. W., Physisorption of gases, with special reference to the evaluation of surface area and pore size distribution (IUPAC Technical Report). *Pure Applied Chemistry* **2015,** *87*.

31. Peacock, A., *Handbook of Polyethylene: Structures, Properties and Applications*. Marcel Dekker, Inc: New York, 2000.

32. Machado, F.; Lima, E. L.; Pinto, J. C.; McKenna, T. F. L., Evaluation of the Initial Stages of Gas-Phase Ethylene Polymerizations with a SiO_2-Supported Ziegler–Natta Catalyst. *Macromolecular Reaction Engineering* **2009,** *3*, 47–57.

33. Tioni, E. Optimization of a tool to study the start-up of the gas phase olefin polymerization. Université de Lyon, Lyon, 2011.

34. Tioni, E.; Monteil, V.; McKenna, T. F. L., Morphological Interpretation of the Evolution of the Thermal Properties of Polyethylene during the Fragmentation of Silica Supported Metallocene Catalysts. *Macromolecules* **2013,** *46* (2), 335-342.

35. Di Martino, A.; Weickert, G.; McKenna, T. F. L., Contributions to the Experimental Investigation of the Nascent Polymerisation of Ethylene on Supported Catalysts, 1. A Quenched-Flow Apparatus for the Study of Particle Morphology and Nascent Polymer Properties. *Macromolecular Reaction Engineering* **2007,** *1*, 165–184.

36. Di Martino, A.; Weickert, G.; McKenna, T. F. L., Contributions to the Experimental Investigation of the Nascent Polymerisation of Ethylene on Supported Catalysts, 2. Influence of Reaction Conditions. *Macromolecular Reaction Engineering* **2007,** *1* (2), 229-242.